Anharmonic phonons of $NaZr_2(PO_4)_3$ studied by Raman spectroscopy, first-principles calculations, and x-ray diffraction

K. Kamali, T. R. Ravindran,* C. Ravi, Y. Sorb, N. Subramanian, and A. K. Arora
Materials Science Group, Indira Gandhi Centre for Atomic Research, Kalpakkam 603 102, India
(Received 28 March 2012; revised manuscript received 19 July 2012; published 1 October 2012)

Raman spectroscopy, x-ray diffraction, and *ab initio* calculations are carried out to gain insight into the thermal expansion properties of $NaZr_2(PO_4)_3$. *In situ* Raman studies at high pressure in a diamond anvil cell indicate that two low-energy phonons corresponding to a combination of PO_4 tetrahedral librations and Zr translations contribute negatively to its thermal expansion, and temperature-dependent Raman studies reveal the modes that are truly anharmonic. To complement the spectroscopic measurements the phonon spectrum is computed and mode assignments are carried out employing first-principles calculations. The computed atomic displacements corresponding to the lowest-energy Raman mode indicates that it involves PO_4 rotations and Zr translations, and its Gruneisen parameter is found to be negative, in agreement with our measured value. The thermal expansion coefficient calculated using mode Gruneisen parameters obtained from computed phonon spectra at different volumes (7.5×10^{-6}/K) is in good agreement with the reported value (4.5×10^{-6}/K). *In situ* x-ray diffraction measurements in a diamond anvil cell are carried out up to 20 GPa. There are clear indications of a phase transformation above 5.5 GPa, and the transformation is reversible with little hysteresis. From our x-ray diffraction measurements and density functional theory calculations the bulk modulus of rhombohedral $NaZr_2(PO_4)_3$ is determined to be 47 and 45 GPa, respectively, and these values are used to obtain the respective Gruneisen parameters.

DOI: 10.1103/PhysRevB.86.144301 PACS number(s): 63.20.Ry, 62.50.−p, 65.40.De, 78.30.−j

I. INTRODUCTION

$NaZr_2(PO_4)_3$ (NZP) is the prototype of a broad family of compounds with a three-dimensional skeletal framework of the form $[A_{2n}(XO_4)_{3n}]^{m-}$ that renders the structure highly stable and flexible.[1] Corner-sharing PO_4 tetrahedra and ZrO_6 octahedra form this framework, with the Na ions placed in the interstitial sites determined by the PO_4 and ZrO_6 polyhedra.[2] The NZP family of compounds are well known for their ultralow thermal expansion properties and superionic conductivity, and they have also been considered as a host for nuclear waste immobilization due to their ability to accommodate most of the radioactive ions of widely different sizes at the interstitial Na sites or at the octahedral Zr sites.[3] High-temperature x-ray diffraction studies and differential thermal analysis on NZP showed the absence of phase transitions up to 1073 K and 898 K, respectively.[4,5] High-pressure x-ray diffraction studies on an isostructural compound $RbTi_2(PO_4)_3$ has revealed a subtle phase transformation from the *R-3c* to *R3* structure at a pressure of 1.7 GPa.[6] However, there are no reports of high-pressure investigations of NZP in the literature.

Study of the thermal expansion of materials has attracted considerable attention in recent times due to the discovery of large and isotropic negative thermal expansion (NTE) in cubic $Zr(WO_4)_2$ over a large temperature range of 0.3–1050 K,[7] an even greater NTE coefficient in cubic $Zn(CN)_2$,[8] and colossal thermal expansion in $Ag_3[Co(CN)_6]$.[9] The mechanism of thermal expansion in such materials has been extensively studied by use of various techniques such as Raman spectroscopy,[10–15] inelastic neutron scattering,[16–19] extended x-ray absorption fine structure,[20] reverse Monte Carlo modeling of neutron total scattering data,[21] specific heat,[22,23] perturbed angular correlation,[24] infrared spectroscopy,[25] and lattice dynamics modeling.[26,27] In $Zr(WO_4)_2$ a low-energy rigid unit mode of WO_4 tetrahedral librations at 41 cm^{-1} has been identified to contribute largely to its NTE, whereas in $Zn(CN)_2$ the librational and translational modes of the rigid C ≡ N unit at 339 cm^{-1} contribute to NTE.[14] Trigonal $Ag_3[Co(CN)_6]$ exhibits positive thermal expansion along the *a* axis and comparable NTE along the *c* axis from 16 to 500 K—its decomposition temperature—but the resultant volume thermal expansion is positive ($\alpha_V = 45 \times 10^{-6}\,K^{-1}$). Recent high-pressure Raman spectroscopic investigations have revealed that Co-CN bending modes that occur at about 335 cm^{-1} are responsible for NTE in $Ag_3[Co(CN)_6]$[15] that is reminiscent of the role of the C ≡ N mode in $Zn(CN)_2$.[14] Cubic ZrV_2O_7 is another network structure that exhibits large and isotropic NTE above 373 K and is structurally related to ZrW_2O_8: The mechanism of NTE is similar in both materials, i.e., coupled rotation of WO_4/VO_4 tetrahedra and ZrO_6 octahedra. Nevertheless, ZrW_2O_8 has only three of the four oxygen atoms of its WO_4 tetrahedra corner-sharing ZrO_6 octahedra, and the terminal oxygen of the tungstate ion along the ⟨111⟩ axis was also reported to play a major role in its NTE.[24] ZrV_2O_7 has each of its VO_4 tetrahedra fully corner shared with three ZrO_6 octahedra and one other VO_4 tetrahedron. Lattice dynamical calculations have shown that the various oxygen atoms in ZrV_2O_7 have nearly the same values of their vibrational amplitudes due to this more rigid framework, whereas in ZrW_2O_8 the oxygen atoms have significantly different vibrational amplitudes, indicating distortions of ZrO_6 octahedral and WO_4 tetrahedral units.[28] In $NaZr_2(PO_4)_3$ each PO_4 tetrahedron is connected to four ZrO_6 octahedra and each ZrO_6 octahedron is connected to six PO_4 tetrahedra; there are no terminal oxygen atoms, similarly to ZrV_2O_7. NZP exhibits anisotropic thermal expansion, with $\alpha_c = 23.5 \times 10^{-6}\,K^{-1}$ and $\alpha_a = -5 \times 10^{-6}\,K^{-1}$, with an overall low positive thermal expansion coefficient of the order $\alpha_{av} = 4.5 \times 10^{-6}\,K^{-1}$ from

293 to1273 K.[29] Dilatometric measurements on a ceramic bar, however, result in a negative bulk thermal expansion coefficient $\alpha_{av} = -0.4 \times 10^{-6}\,K^{-1}$ over the temperature range of 298–773 K.[30] The apparent (bulk) values of the thermal expansion coefficient, in general, are lower than the intrinsic values determined from x-ray diffraction since part of the expansion could take place in micro cracks in the material.[31]

Thermal expansion in solids arises from anharmonic lattice vibrations. Change in phonon frequency as a function of temperature is due to two contributions that could be decoupled: a quasiharmonic contribution due to change in lattice volume (also known as the *implicit contribution*) and the other, purely anharmonic (explicit), contribution due to change in vibrational amplitude.[32]

The purpose of the current study is twofold: to investigate the contribution of the various phonon modes to the thermal expansion of NZP through experiments and *ab initio* calculations and to investigate its structural stability at high pressures. Raman spectroscopic studies as a function of pressure at ambient temperature and as a function of temperature at ambient pressure were performed to identify the anharmonic phonons. High-pressure x-ray diffraction measurements were carried out to determine the structural stability of NZP and its equation of state. To complement the Raman and x-ray diffraction (XRD) studies, the P-V equation of state, phonon dispersion, and the characters of irreducible representation were computed via density functional theory (DFT) and density functional perturbation theory (DFPT) calculations, using the Vienna *ab initio* simulation package (VASP) and PHONOPY. The thermal expansion coefficient was calculated from Gruneisen parameters of all phonons and compared with the reported value.

II. EXPERIMENTAL AND COMPUTATIONAL DETAILS

$NaZr_2(PO_4)_3$ was synthesized by mixing stoichiometric amounts of precursor solutions of 1 M NaCl, 1.5 M $ZrOCl_2$, and 6 M H_3PO_4 following the procedure of Agarwal and Adair.[33] This viscous slurry was heated at 70 °C for 24 h. The resulting gel was dried at 150 °C for 4 h and ground, calcined at 700 °C for 16 h, and then, finally, heat treated at 1100 °C for 24 h. The final product is fine white polycrystalline powder whose XRD pattern matched with the JCPDS pattern [PDF NO: 33-1312] without any impurity peaks.

In situ high-pressure Raman spectra were recorded up to ∼20 GPa from a symmetric diamond anvil cell (DAC) with diamonds of culet diameter 500 μm, using a micro Raman spectrometer (Renishaw, UK, model Invia) with 514-nm laser excitation. The sample was loaded along with ruby pressure calibrant and a 4:1 mixture of methanol-ethanol medium into a 200-μm hole drilled into a preindented stainless steel gasket. The spectra were recorded in both increasing and decreasing pressure cycles. Temperature-dependent Raman measurements from 80 to 860 K were carried out using a heating and cooling microscope stage (Linkam THMS 600).

High-pressure x-ray diffraction experiments were carried out at ambient temperature using a Mao-Bell–type DAC with diamonds of 600-μm culet diameter in an angle dispersive mode at several pressures up to ∼19 GPa. The powdered sample was loaded along with methanol-ethanol medium and gold powder for pressure calibration into a 200-μm-diameter hole drilled in a stainless steel gasket. The Mo K_α x-ray beam was incident from a Rigaku ULTRAX (18 kW) rotating anode x-ray generator with a graphite monochromator. The overall resolution of the diffractometer is $\delta d/d \sim 0.001$. An image plate based mardtb345 diffractometer was used. The sample-to-detector distance was calibrated using a standard LaB_6 specimen. Two-dimensional image data from the Mar345IP detector were converted to intensity versus 2θ using the FIT2D program. The high-pressure XRD patterns were indexed with the POWD program,[34] and the lattice parameter was refined by least-squares fitting using AIDS 83 software.

Theoretical calculation of the phonon spectrum was carried out using VASP.[35–37] VASP performs an iterative solution of the Kohn-Sham equations in a plane-wave basis. First, full structural relaxations of the 36-atom rhombohedral primitive unit cell of $NaZr_2(PO_4)_3$ [space group *R-3c* (167)][38] were carried out. The interaction of valence electrons with ionic cores is represented by the ultrasoft pseudopotentials.[39] Electronic exchange and correlation are described by the gradient-corrected PW91 functional.[40] A plane-wave cut-off energy of 500 eV was used. Brillouin-zone integrations were performed on a $7 \times 7 \times 7$ Γ-centered Monkhorst-Pack[41] grid, with a Gaussian smearing width of $\sigma = 0.05$. Ionic relaxation was stopped when all forces were smaller than 1×10^{-6} eV/Å. Next, with the equilibrium geometry obtained from the first step, VASP was restarted with DFPT[42,43] flag turned on (IBRION = 8) and the response function calculations were carried out in order to obtain the first derivatives of the occupied wave functions with respect to the perturbations of atomic displacements. This was then used to compute the force-constant Hessian matrix, the elementary second derivative response-function tensors.[44,45] Using DFPT, VASP determines the Hessian matrix for wave vector $q = 0$ and computes zone-centered phonon frequencies and eigenvectors. For computing the phonon spectrum over the entire Brillouin zone, the PHONOPY program[46] was used. PHONOPY reads the Hessian matrix of VASP calculations and interpolates over the first Brillouin zone for the specified q grid. To verify the convergence of the DFPT calculations, we also computed the phonon spectrum of NZP with a 108-atom hexagonal close-packed unit cell and found that the zone center phonon modes varied by only a few THz. Visual representations of the different phonon modes were obtained by plotting the eigenvectors of displacement of the various atoms in the unit cell using VESTA visualization software.[47]

III. RESULTS AND DISCUSSION

$NaZr_2(PO_4)_3$ crystallizes in a rhombohedral structure with space group *R-3c* (D_{3d}^6) with six formula units in the crystallographic unit cell. The Na, Zr, P, and O atoms sit at Wyckoff sites *b*, *c*, *e*, and *f*, respectively.[2] The two formula units in the primitive cell give rise to 108 degrees of freedom. We carried out factor group analysis by use of the Halford-Hornig site group method[48] to obtain the irreducible representation $\Gamma_{\text{Total}} = 8A_{1g} + 9A_{2g} + 17E_g + 9A_{1u} + 10A_{2u} + 19E_u$. This is further classified into internal modes of phosphate ions and lattice modes:

$\Gamma_{Int} = 5A_{1g} + 4A_{2g} + 9E_g + 5A_{1u} + 4A_{2u} + 9E_u$ (with $\nu_1 = A_{1g} + E_g + A_{1u} + E_u$; $\nu_2 = 2A_{1g} + 2E_g + 2A_{1u} + 2E_u$; ν_3 and $\nu_4 = A_{1g} + 2A_{2g} + 3E_g + A_{1u} + 2A_{2u} + 3E_u$); $\Gamma_{Ext} = 3A_{1g} + 5A_{2g} + 8E_g + 4A_{1u} + 6A_{2u} + 10E_u$ (24 translational modes: $\Gamma(Na)^{Trans} = A_{1u} + A_{2u} + 2E_u$; $\Gamma(Zr)^{Trans} = A_{1g} + A_{2g} + 2E_g + A_{1u} + A_{2u} + 2E_u$; $\Gamma(PO_4)^{Trans} = A_{1g} + 2A_{2g} + 3E_g + A_{1u} + 2A_{2u} + 3E_u$ and 12 librational modes $\Gamma(PO_4)^{Libr} = A_{1g} + 2A_{2g} + 3E_g + A_{1u} + 2A_{2u} + 3E_u$); $\Gamma_{Acoustic} = A_{2u} + E_u$; A_{2g} and A_{1u} modes are optically inactive. There are, in total, 25 Raman active modes ($18A_{1g}$ and $17E_g$) and 27 IR active modes ($9A_{2u}$ and $18E_u$) expected.

A. Raman spectroscopic and computational studies

The Raman spectrum of NZP at ambient conditions exhibits 17 distinct Raman bands (Fig. 1 and Table I), similarly to that reported earlier.[49] Observation of a smaller number of modes could be due to accidental degeneracies or insufficient intensities arising from small polarizability of some of the modes. Raman bands in the range 325–1084 cm^{-1} arise from the internal vibrations of phosphate ions, and one expects the most intense band at 1026 cm^{-1} to be the symmetric stretch mode. Lattice modes below 270 cm^{-1} arise from the translations of the Zr and the translations and librations of the PO_4 ions.[49,50]

In the absence of polarized Raman measurements on single crystals, *ab initio* calculations have emerged as an alternative to carry out mode assignments. Eigenfrequencies for the various modes of NZP were obtained by diagonalizing the dynamical matrix. The computed phonon dispersion at equilibrium volume (528.66 $Å^3$) is shown in Fig. 2. The zone-center phonon frequencies are compared with experimental values in Table I. The total irreducible representation obtained from computations is consistent with the results of group theoretical analysis detailed above. Mode assignments were obtained from the VASP-computed eigenvectors using the PHONOPY program, and Raman mode frequencies closest to the computed values were assigned the corresponding symmetry species, excluding the Raman inactive mode A_{2g}. The two lowest-energy optical modes are found to be E_u (infrared active) modes at 71 and 76 cm^{-1}, and the first E_g band is at 113 cm^{-1}, the corresponding experimental value of Raman shift being 72 cm^{-1}. We find closer matching of computed and experimental values for several other modes except the ν_1 and ν_3 internal modes of PO_4 above 1000 cm^{-1}. It turns out (see later) that the E_g band at 72 cm^{-1} (experimental) is highly anharmonic. The difference between the experimental and computed frequencies for this mode could be due to the harmonic approximation of our lattice dynamic calculations. In order to see if better matching with experimental frequencies could be obtained, we also carried out calculations using

TABLE I. Frequencies and Gruneisen parameters (γ_i) of Raman modes of NZP from experiments and simulations. Mode assignments were obtained from the VASP computed eigenvectors using the PHONOPY program.

Experimental		DFPT		
ω (cm^{-1})	γ_i	ω (cm^{-1})	γ_i	Mode Assignments
72	−2.26	113	−2.61	E_g
112	−0.64	127	5.08	E_g
126	0.19	141	2.74	A_{1g}
139	0.59	157	1.08	E_g
154	0.85	166	2.23	E_g
192	0.43	185	4.31	A_{1g}
262	0.24	273	0.39	E_g
293	0.30	298	1.60	A_{1g}
325	0.66	337	0.50	E_g
422	0.12	425	0.37	E_g
435	0.32	431	0.62	A_{1g}
595	0.15	577	0.18	A_{1g}
642	0.24	623	0.20	E_g
1026	0.19	927	0.60	E_g
1040	0.29	947	0.62	A_{1g}
1061	0.22	991	0.43	E_g
1081	0.18	1018	0.25	A_{1g}

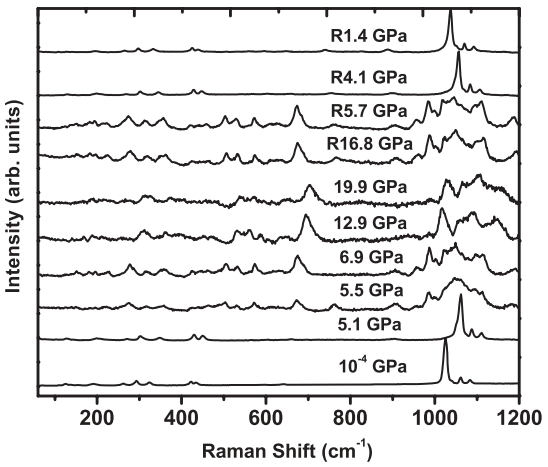

FIG. 1. Raman spectra of NZP at different pressures. The three spectra at the top are in the pressure reducing run. There is a dramatic change in the spectra at 5.5 GPa, and the change is reversible on reducing the pressure.

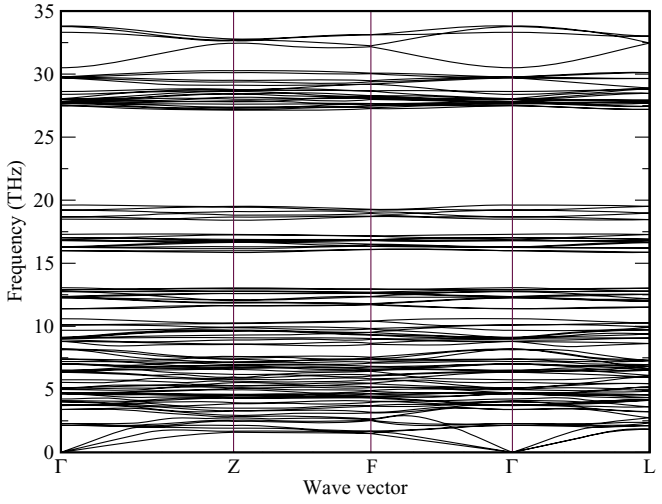

FIG. 2. (Color online) Phonon dispersion curves of $NaZr_2(PO_4)_3$ from DFPT calculations using VASP with the 36 atom rhombohedral primitive unit cell. The E_g zone center phonon frequencies exhibit good matching with experimental Raman values.

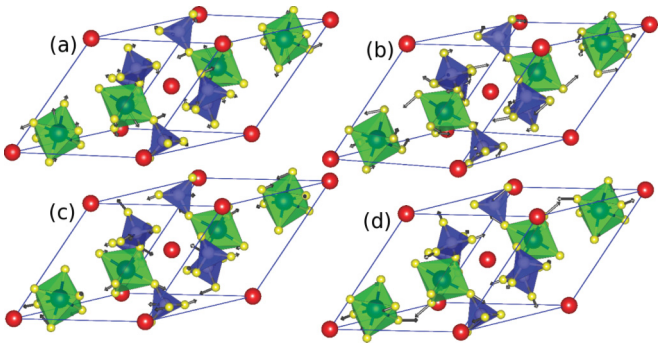

FIG. 3. (Color online) Atomic displacements of (a) the 113-cm^{-1} mode showing a combination of the PO_4 librations and Zr translations, (b) the 127-cm^{-1} mode exhibiting coupled rotation of PO_4 tetrahedra and ZrO_6 octahedra, (c) the asymmetric stretch mode of PO_4 at 927 cm^{-1} corresponding to the most intense Raman band at 1026 cm^{-1}, and (d) symmetric stretch mode of PO_4 at 991 cm^{-1} corresponding to the Raman band at 1061 cm^{-1}.

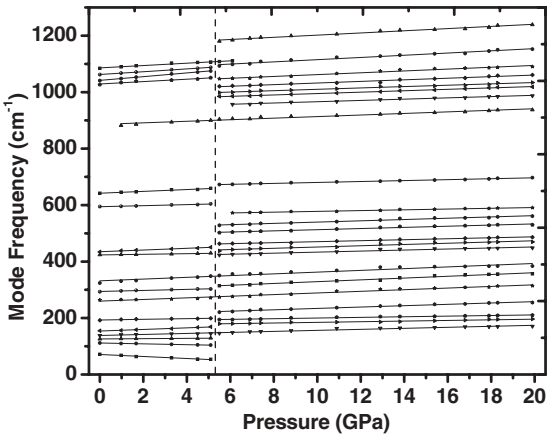

FIG. 4. ω vs P of NZP. Changes in the spectral frequencies are clearly seen at 5.5 GPa, signifying a phase transformation that is confirmed from XRD measurements.

projector augmented-wave (PAW) pseudopotentials; the corresponding zone center E_g mode frequency is 81 cm^{-1}, which is closer to the experimental value of 72 cm^{-1}; however, when the PAW-based dynamical matrix was employed to compute the phonon frequencies over the entire Brillouin zone, imaginary frequencies were obtained over the F-Γ segment. Therefore, we worked with ultrasoft pseudopotentials that eliminated unphysical frequencies.

Atomic displacement plots of the lowest-energy (IR active E_u) modes at 71 and 76 cm^{-1} using the VESTA program reveal them to be translational modes of Na atoms. Figure 3 shows the displacement vectors for the two lowest-energy Raman modes and two of the internal modes of the PO_4 ion: The E_g mode at 113 cm^{-1} [Fig. 3(a)] is seen to be a combination of the PO_4 librations and Zr translations that contribute negatively to thermal expansion–consistent with the present experimental and computational results (Table I) and similar to the role played by WO_4 in $Zr(WO_4)_2$ and C ≡ N in $Zn(CN)_2$.[12,14] The E_g mode at 127 cm^{-1} [Fig. 3(b)] seems to exhibit coupled rotation of PO_4 tetrahedra and ZrO_6 octahedra. The Gruneisen parameter of this mode is experimentally determined to be negative (Table I). The PO_4 ion's internal mode at 927 cm^{-1}, corresponding to the most intense Raman band at 1026 cm^{-1} [Fig. 3(c)], is found to be an asymmetric stretch mode, consistent with the assignment (ν_3) of Barj *et al*.[49] Another internal mode at 991 cm^{-1}, corresponding to the Raman band at 1061 cm^{-1} [Fig. 3(d)], exhibits symmetric stretch of two of the six PO_4 tetrahedra in the unit cell. This could be assigned as the ν_1 mode, contrary to the assignment by Barj *et al*.[49]

From Raman spectroscopic measurements, it is seen that, as the pressure is increased, the low-energy bands at 72 cm^{-1} and 112 cm^{-1}, which arise from PO_4 librations and Zr translations, soften and the intensity of the 595-cm^{-1} band weakens gradually. There are distinct changes in the spectra above 5.5 GPa, as also observed in the ω vs. P plot (Fig. 4): (i) three Raman bands below 130 cm^{-1}, viz., 72, 112, and 126 cm^{-1} disappear; (ii) the intensity of the symmetric stretch mode reduces dramatically, there is a merger of nearby modes leading to a broad feature about 1050 cm^{-1}, and several mode frequencies in this region are down shifted; (iii) the intensities of bands at 274, 672, 891, and 985 cm^{-1} increase (with the band at 891 cm^{-1} appearing from 1.6 GPa itself); (iv) many distinct peaks appear in the region of 100–1200 cm^{-1} (such as 505, 532, 573, 957, 987, and 1025 cm^{-1}) above 5.5 GPa. These are clear indications of a structural phase transformation about 6 GPa from rhombohedral (phase I) to a new phase (phase II). There are no distinct changes in the spectra of phase II up to 20 GPa, the highest pressure in the present study. These results indicate that the high-pressure phase is stable up to 20 GPa compared to other NTE framework structures that exhibit irreversible pressure-induced amorphization.[10,51–55] It is also found that the phase transition around 5.5 GPa is reversible: Spectra were recorded at 10 different pressures in the decreasing pressure cycle, and phase I is recovered with negligible hysteresis (Fig. 1). The number of Raman bands in phase II is more than that in phase I, indicating that the structure has transformed to one of lower symmetry. The reduction of frequency of the symmetric stretching mode in phase II corresponds to a decrease in the force constant. This decrease might be due to a distortion of bonds in the PO_4 units that can occur due to the rearrangement of the tetrahedra to accommodate the change in volume.[56] Table I lists the mode frequencies (ω_i) and the corresponding Gruneisen parameters [$\gamma_i = (B_0/\omega_i)(d\omega_i/dP)$], where B_0 is the bulk modulus obtained from high-pressure XRD measurements described later. Gruneisen parameters for several internal modes are significantly positive, which indicates that these modes contribute positively to thermal expansion (PTE). The negative contribution to thermal expansion is by the two low-frequency modes at 72 and 112 cm^{-1} that correspond to librations of PO_4 tetrahedra and Zr translation, respectively,[50] reminiscent of other NTE systems such as $Zr(WO_4)_2$ and $Zn(CN)_2$.[12,14]

The phonon spectrum was computed at a lower volume of 512.96 $Å^3$ (corresponding to 2.65 GPa) in addition to that at equilibrium volume. The Γ-point phonon frequencies at this volume and the equilibrium volume were employed to obtain the mode Gruneisen parameters using the expression $\gamma_i = -\frac{V_{eq}}{\omega_i}\frac{\Delta\omega_i}{\Delta V}$. The mode Gruneisen parameters γ_i for all 70 optical modes, except the lowest energy Raman active E_g band

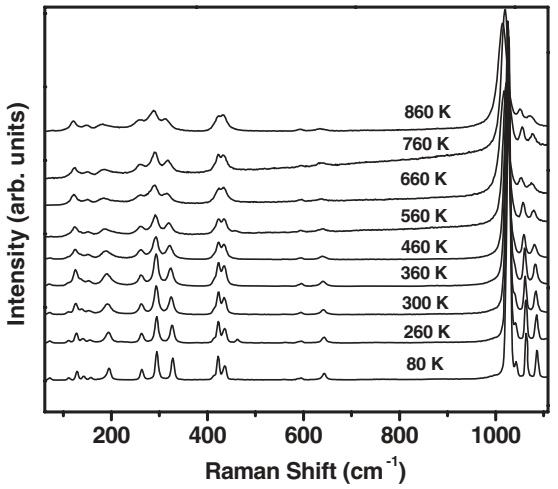

FIG. 5. Raman spectra of NZP at different temperatures. The compound is stable in the entire temperature range from 80 K to 860 K.

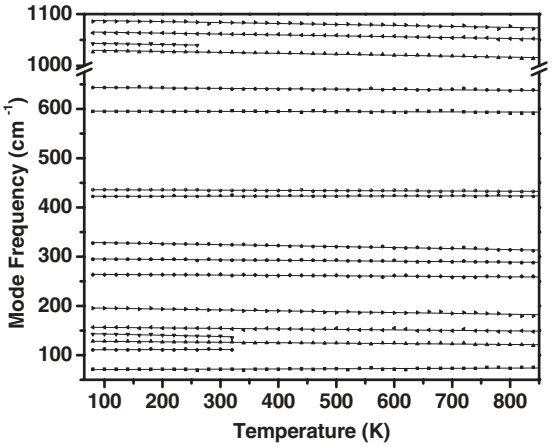

FIG. 6. ω vs T of NZP showing monotonic decrease in the mode frequencies of all modes except the two lowest, at 72 and 110 cm^{-1}, which exhibit opposite behavior.

($\omega_{calculated} = 113$ cm^{-1}, $\omega_{experimental} = 72$ cm^{-1}) mentioned above, are positive, whereas experimentally, the next higher energy E_g mode ($\omega_{calculated} = 124$ cm^{-1}, $\omega_{experimental} = 112$ cm^{-1}) also is found to be negative. The close matching of γ_i for this mode is fortuitous, considering the extent of mismatch for other modes. Table I shows a comparison of the computed and experimental mode Gruneisen parameters for the 17 observed Raman modes. Using Einstein's specific heat $C_i = R[x_i^2 \exp(x_i)]/[\exp(x_i) - 1]^2$, where $x_i = \hbar\omega_i/k_BT$, for the various modes ($i = 1$ to 70) the total specific heat C_V was obtained. Here R is the universal gas constant. The thermal expansion coefficient $\alpha = (\gamma_{av}C_V)/(3V_mB_0)$, where $\gamma_{av} = \frac{1}{2}\sum p_iC_i\gamma_i/C_V$, p_i are the degeneracies of the respective ω_i phonon branches at the Brillouin zone center, and V_m is the molar volume. The bulk modulus B_0 was computed by fitting the DFT calculated energy vs volume data to the Vinet universal equation of state.[57] Our calculations involve a set of seven energy-volume data over the range of XRD pressures and we find that the calculated bulk modulus of 44.7 GPa is in good agreement with 47 ± 5 GPa obtained from high-pressure XRD measurements. The equilibrium volume V_m is determined to be 3.2×10^{-4} m^3/mole, and the calculated value of $\alpha = 7.5 \times 10^{-6}$ K^{-1} is in good agreement with the reported value of 4.5×10^{-6}/K.

Figure 5 shows the Raman spectra of NZP at different temperatures over the complete range of phonon frequencies. Frequencies of most of the modes decrease as a function of temperature, but the modes at 72 and 112 cm^{-1} exhibit opposite behavior. No discontinuous changes are noted, indicating the absence of any phase transition that also agrees with high-temperature XRD results.[28] $d\omega_i/dT$ of the various phonon frequencies were obtained by linear fits to ω vs T

TABLE II. Total anharmonicities and quasiharmonic and true anharmonic contributions of different phonons in NZP. The numbers in the parentheses are standard errors to the least significant digit.

Mode frequencies (cm^{-1})	Total anharmonic (10^{-5} K^{-1})	Quasiharmonic $\alpha\gamma_j$ (10^{-5} K^{-1})	True anharmonic (10^{-5} K^{-1})
72	5.9(3)	− 1.0(2)	4.9
110	1.7(3)	− 0.2(9)	1.6(2)
126	− 7.1(9)	0.08(5)	− 7.1
139	− 10.9(3)	0.2(6)	− 10.7(5)
154	− 6.5(3)	0.3(8)	− 6.1(5)
192	− 9.1(9)	0.1(9)	− 9.0(6)
262	− 2.7(4)	0.1(1)	− 2.6(2)
293	− 3.0(9)	0.1(4)	− 2.9(5)
325	− 6.1(1)	0.2(9)	− 5.8(2)
422	0.2(7)	0.05(4)	0.3(3)
435	− 0.9(7)	0.1(4)	− 0.8(3)
595	− 0.4(4)	0.06(8)	− 0.3(7)
642	− 1.1(1)	0.1(1)	− 1.0(3)
1026	− 1.7(8)	0.08(6)	− 1.6(8)
1040	− 1.7(6)	0.1(3)	− 1.6(2)
1061	− 1.6(2)	0.09(9)	− 1.5(2)
1084	− 1.7(2)	0.08(1)	− 1.6(3)

(Fig. 6). These numbers represent the total anharmonicities of the modes. Separation of true anharmonic and quasiharmonic parts was effected using the well-known formula[32]

$$\frac{1}{\omega_i}\frac{d\omega_i}{dT}\bigg|_P = \frac{1}{\omega_i}\frac{\partial\omega_i}{\partial T}\bigg|_V - \gamma_i\alpha,$$

where the first term on the right-hand side is the true anharmonic (intrinsic) contribution, and the second, quasiharmonic term. Using the present mode Gruneisen parameters γ_i and thermal expansion coefficient $\alpha = 4.5 \times 10^{-6}$ K^{-1}, we obtain the anharmonicities of 17 of the 27 modes at 80 K (Table II). The magnitude of anharmonicity of these modes is almost an order of magnitude less compared to zirconium tungstate[13] which indicates lower contribution to thermal expansion. The values of true anharmonicities for all modes except 72, 112, and 422 cm $^{-1}$ are negative. The magnitude of intrinsic (true) anharmonicity is higher for low frequency modes (especially for modes at 126, 139, 154, 192, and 325 cm^{-1}) compared to the high frequency modes which agrees well with the fact that the internal modes are harder compared to the low frequency modes. Table II also shows that quasiharmonic (implicit) contribution for all modes are small; thus, the true anharmonicities are nearly the same as the total anharmonicities. It also signifies the little change in lattice volume with an increase in temperature so the modes remain stable and intact without any phase transition due to small values of implicit contribution.

B. High pressure x-ray diffraction

We have performed *in situ* high-pressure x-ray diffraction measurements on NZP to obtain the bulk modulus and to confirm the phase transformation indicated by Raman spectroscopy. The lattice parameters of the hexagonal unit cell [$a = 8.806(1)$, $c = 22.757(6)$] obtained from the ambient pressure data are in good agreement with those reported in the literature.[58] XRD patterns at several different pressures (Fig. 7) were analyzed using POWD software. Up to 4.8 GPa the patterns could be indexed with a good figure of merit of 11

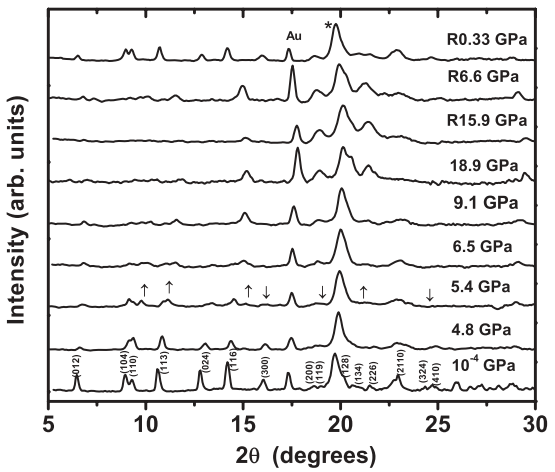

FIG. 7. XRD patterns at different pressures. The asterisk denotes a gasket peak and Au the pressure marker. Disappearance of several reflections is noticeable above 6 GPa. Patterns recorded in the pressure reducing cycle are indicated by the prefix "R."

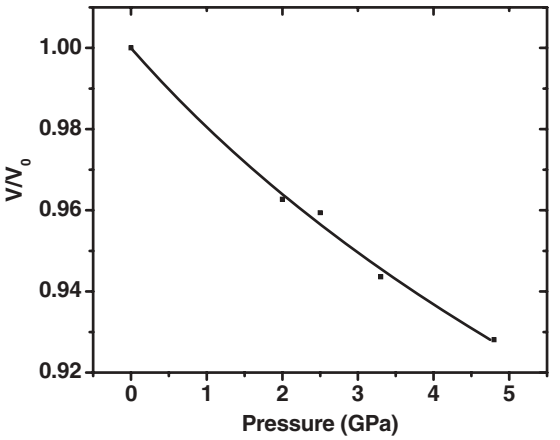

FIG. 8. Pressure vs reduced volume of the hexagonal phase of NZP up to 5 GPa. Data fitted to a third-order Birch-Murnaghan equation result in $B_0 = 47 \pm 5$ GPa and $B_0' = 8 \pm 4$.

to a hexagonal structure *R-3c* with monotonically decreasing volume. Several new peaks (at $2\theta = 9.8°$, $11.2°$, $15.1°$, $21.1°$) emerge around 5.4 GPa, and some old peaks ($2\theta = 16.1°$, $24.9°$) disappear, and the pattern differs substantially from the starting phase around 9.1 GPa. The quality of XRD patterns in this high-pressure phase does not permit us to unambiguously determine its structure. Lattice parameters and the corresponding volumes up to 5 GPa are shown in Figs. 8 and 9. When the P vs V in the hexagonal phase is fitted to a third-order Birch-Murnaghan equation,[59] a bulk modulus value B_0 of 47 ± 5 GPa and $B_0' = 8 \pm 4$ are obtained (Fig. 8). On decompression the XRD patterns corresponding to the original phase are obtained (Fig. 7), indicating the reversibility of the phase transformation.

High-pressure studies on flexible materials such as SiO_2 and GeO_2 with α-quartz structure indicate large compressibilities without much variation in bond lengths. There are large changes in bond angles but there is no bond breaking; tilting and rotation of polyhedral units help the structures remain stable.[60] The recently reported $Ag_3[Co(CN)_6]$ framework structure shows irreversible structural phase transition (from trigonal to a monoclinic structure) at a low pressure of about 0.2

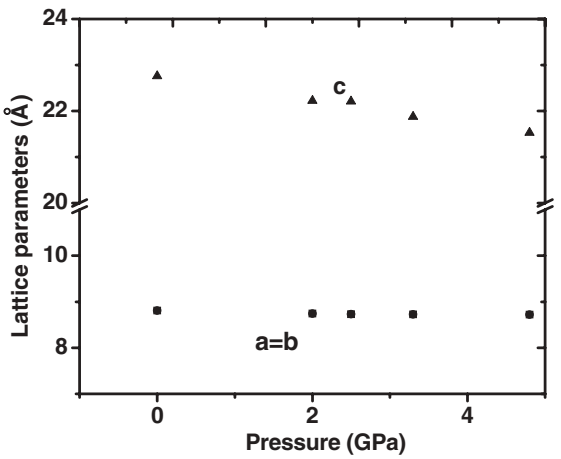

FIG. 9. Unit cell parameters of NZP at different pressures. The errors in the data are less than the height of the symbols.

GPa.[61] An earlier high-pressure XRD study[6] on $RbTi_2(PO_4)_3$ also showed an isostructural phase transformation (from *R-3c* to *R-3*) due to the distortion of Ti-P framework that causes the interstitial cavities to collapse around the larger rubidium cation with an increase in coordination of the cation. From the present results, we conclude that a reversible phase transformation occurs around 6 GPa and this phase continues to exist at least up to 20 GPa.

IV. SUMMARY AND CONCLUSION

Thermal expansion behavior of $NaZr_2(PO_4)_3$ is investigated using Raman spectroscopy as a function of temperature at ambient pressure and as a function of pressure at ambient temperature. From an analysis of these results the anharmonicity of the various phonon modes are obtained; the individual modes that make negative and positive contributions to thermal expansion in this material are identified, indicating that the PO_4 tetrahedral librations and Zr translations contribute to negative thermal expansion. We find indications of phase transformation from our high-pressure Raman studies. Our x-ray diffraction measurements also show a reversible phase transformation around 6 GPa, in accordance with Raman spectroscopic observations. The new structure is found to remain stable up to 20 GPa, in contrast to other related framework structures that exhibit negative thermal expansion and pressure-induced amorphization. Density functional perturbation theoretical calculations of phonon spectrum of NZP were carried out using VASP code. Mode assignments were carried out using PHONOPY combined with VASP computed zone-center phonon frequencies and eigenvectors. From our first-principles equation-of-state calculations at several pressures from ambient to 5 GPa, we find that $NaZr_2(PO_4)_3$ has a bulk modulus of 45 GPa, in agreement with the measured value of 47 GPa. The thermal expansion coefficient obtained from the calculated phonon mode frequencies at different volumes is in good agreement with the reported experimental value.

ACKNOWLEDGMENTS

We thank V. Sivasubramanian, V. Sridharan, and R. Nithya for fruitful discussions, B. V. R. Tata for interest in the work, M. C. Valsakumar and C. S. Sundar for encouragement, and S. C. Chetal for support. N.S. wishes to thank colleagues in the High Pressure Physics Section for help in experimental work.

*Corresponding author: trr@igcar.gov.in

[1] J. Alamo, Solid State Ionics **63**, 547 (1993).
[2] D. K. Agarwal, C. Y. Huang, and H. A. McKinstry, Int. J. Thermophys. **12**, 4 (1991).
[3] B. E. Scheetz, D. K. Agarwal, E. Breval, and R. Roy, Waste Management **14**, 489 (1994).
[4] V. I. Petkov, A. I. Orlavo, G. N. Kasantsev, S. G. Samoilov, and M. L. Spiridonova, J. Therm. Anal. Cal. **66**, 623 (2001).
[5] V. I. Petkov, E. A. Asabina, A. V. Markin, N. N. Smirnova, and D. B. Kitaev, J. Therm. Anal. Cal. **80**, 695 (2005).
[6] R. M. Hazen, D. C. Palmer, L. W. Finger, and G. D. Stucky, J. Phys.: Condens. Matter **6**, 1333 (1994).
[7] T. A. Mary, J. S. O. Evans, T. Vogt, and A. W. Sleight, Science **272**, 90 (1996).
[8] D. J. Williams, D. E. Partin, F. J. Lincoln, J. Kouvetakis, and M. O'Keefe, J. Solid State Chem. **134**, 164 (1997).
[9] A. L. Goodwin, M. Calleja, M. J. Conterio, M. T. Dove, J. S. O. Evans, D. A. Keen, L. Peters, and M. G. Tucker, Science **319**, 794 (2008).
[10] T. R. Ravindran, A. K. Arora, and T. A. Mary, Phys. Rev. Lett. **84**, 3879 (2000).
[11] T. R. Ravindran and A. K. Arora, Phys. Rev. Lett. **86**, 4977 (2001).
[12] T. R. Ravindran, A. K. Arora, and T. A. Mary, J. Phys.: Condens. Matter **13**, 11573 (2001).
[13] T. R. Ravindran, A. K. Arora, and T. A. Mary, Phys. Rev. B **67**, 064301 (2003).
[14] T. R. Ravindran, A. K. Arora, S. Chandra, M. C. Valsakumar, and N. V. Chandra Shekar, Phys. Rev. B **76**, 054302 (2007).
[15] R. Rao, S. N. Achary, A. K. Tyagi, and T. Sakuntala, Phys. Rev. B **84**, 054107 (2011).
[16] R. Mittal, S. L. Chaplot, H. Schober, and T. A. Mary, Phys. Rev. Lett. **86**, 4692 (2001).
[17] R. Mittal, S. L. Chaplot, H. Schober, A. I. Kolesnikov, C. K. Loong, C. Lind, and A. P. Wilkinson, Phys. Rev. B **70**, 214303 (2004).
[18] R. Mittal, S. L. Chaplot, and H. Schober, Appl. Phys. Lett. **95**, 201901 (2009).
[19] G. Ernst, C. Broholm, G. R. Kowach, and A. P. Ramirez, Nature **396**, 147 (1998).
[20] D. Cao, F. Bridges, G. R. Kowach, and A. P. Ramirez, Phys. Rev. Lett. **89**, 215902 (2002).
[21] M. G. Tucker, A. L. Goodwin, M. T. Dove, D. A. Keen, S. A. Wells, and J. S. O. Evans, Phys. Rev. Lett. **95**, 255501 (2005).
[22] A. P. Ramirez and G. R. Kowach, Phys. Rev. Lett. **80**, 4903 (1998).
[23] Y. Yamamura, N. Nakajima, T. Tsuji, M. Koyano, Y. Iwasa, S. Katayama, K. Saito, and M. Sorai, Phys. Rev. B **66**, 014301 (2002).
[24] R. Govindaraj, C. S. Sundar, and A. K. Arora, Phys. Rev. B **76**, 012104 (2007).
[25] J. N. Hancock, C. Turpen, Z. Schlesinger, G. R. Kowach, and A. P. Ramirez, Phys. Rev. Lett. **93**, 225501 (2004).
[26] R. Mittal, S. L. Chaplot, and N. Choudhury, Prog. Mater. Sci. **51**, 211 (2006).
[27] R. Mittal and S. L. Chaplot, Phys. Rev. B **60**, 7234 (1999).
[28] R. Mittal and S. L. Chaplot, Phys. Rev. B **78**, 174303 (2008).
[29] T. Ota and I. Yamai, J. Ceram. Soc. Jpn. **95**, 531 (1987).
[30] K. V. G. Kutty, R. Asuvatharaman, C. K. Mathews, and U. V. Varadaraju, Mater. Res. Bull. **29**, 1009 (1994).
[31] I. J. Kim and G. Cao, J. Eur. Ceram. Soc. **22**, 2627 (2002).
[32] B. A. Weinstein and R. Zallen, in *Light Scattering in Solids IV*, edited by M. Cardona and G. Guntherodt (Springer-Verlag, Berlin, 1984), p. 463.
[33] D. K. Agarwal and J. H. Adair, J. Am. Ceram. Soc. **73**, 2153 (1990).
[34] E. Wu, J. Appl. Cryst. **22**, 506 (1989).
[35] G. Kresse and J. Hafner, Phys Rev. B **47**, 558 (1993).

[36]G. Kresse and J. Hafner, Phys. Rev. B **49**, 14251 (1994).
[37]G. Kresse and J. Furthmuller, Phys. Rev. B **54**, 11169 (1996).
[38]L. O. Hagman and P. Kierkegaard, Acta Chem. Scand. **22**, 1822 (1968).
[39]D. Vanderbilt, Phys. Rev. B **41**, 7892 (1990).
[40]J. P. Perdew, J. A. Chevary, S. H. Vosko, K. A. Jackson, M. R. Pederson, D. J. Singh, and C. Fiolhais, Phys. Rev. B **46**, 6671 (1992).
[41]H. J. Monkhorst and J. D. Pack, Phys. Rev. B **13**, 5188 (1976).
[42]X. Gonze and C. Lee, Phys. Rev. B **55**, 10355 (1997).
[43]S. Baroni, S. de Gironcoli, and A. D. Corso, Rev. Mod. Phys. **73**, 515 (2001).
[44]X. Wu, D. Vanderbilt, and D. R. Hamann, Phys. Rev. B **72**, 035105 (2005).
[45]D. Karhanek, T. Bucko, and J. Hafner, J. Phys.: Condens. Matter **22**, 265006 (2010).
[46]A. Togo, F. Oba, and I. Tanaka, Phys. Rev. B **78**, 134106 (2008).
[47]K. Momma and F. Izumi, J. Appl. Crystallogr. **41**, 653 (2008).
[48]W. G. Fateley and F. R. Dollish, *Infrared and Raman Selection Rules for Molecular and Lattice Vibrations* (Wiley-Interscience, New York, 1972).
[49]M. Barj, H. Perthuis, and Ph. Colomban, Solid State Ionics **11**, 157 (1983).
[50]P. Tarte, A. Rulmont, and C. M. Ansay, Spectrochemica Acta A **42**, 1009 (1986).
[51]C. A. Perottoni and J. A. H. Jornada, Science **280**, 886 (1998).
[52]H. K. Poswal, A. K. Tyagi, A. Lausi, S. K. Deb, and S. M. Sharma, J. Solid State Chem. **182**, 136 (2009).
[53]A. K. Arora, R. Nithya, T. Yagi, N. Miyajima and T. A. Mary, Solid State Commun. **129**, 9 (2004).
[54]T. Sakuntala, A. K. Arora, V. Sivasubramanian, R. Rao, S. Kalavathi, and S. K. Deb, Phys. Rev. B **75**, 174119 (2007).
[55]R. Rao, Alka. G. Garg, and T. Sakuntala, J. Appl. Phys. **108**, 083508 (2010).
[56]N. Chandrabhas and A. K. Sood, Phys. Rev. B **51**, 14 (1995).
[57]P. Vinet, J. H. Rose, F. Ferrante, and J. R. Smith, J. Phys.: Condens. Matter **1**, 1941 (1989).
[58]H. Y. P. Hong, Mater. Res. Bull. **11**, 173 (1976).
[59]F. Birch, J. Geophys. Res. **83**, 1257 (1978).
[60]L. Cartz and J. D. Jorgensen, J. Appl. Phys. **52**, 236 (1981).
[61]A. L. Goodwin, D. A. Keen, and M. G. Tucker, Proc. Natl. Acad. Sci. USA **105**, 18708 (2008).